GEOPHYSICS, VOL. 70, NO. 6 (NOVEMBER-DECEMBER 2005); P. G135–G142, 10 FIGS.
10.1190/1.2122412

Depth of investigation for small broadband electromagnetic sensors

Haoping Huang[1]

ABSTRACT

The depth of investigation in electromagnetic (EM) soundings is a maximum depth at which a given target in a given host can be detected by a given sensor. It is of primary interest in EM exploration, particularly for small EM sensors having negligible separation between the transmitter and receiver coils. The depth of investigation is related to many factors, such as sensor sensitivity, precision, operating frequencies, ambient noise level, target and host properties, and the techniques used in data processing and interpretation. Quantitative understanding of the relationships between the depth of investigation and these factors will help users meet their geologic objectives, avoid unnecessary survey expenses, and display meaningful geologic features.

Simple equations to estimate the depth of investigation for handheld EM sensors have been derived from analyzing the EM response based on layered half-space models. The results show that the depth of investigation is approximately proportional to the square root of the skin depth in the host for a given detection threshold and conductivity contrast between the target and host. For a given skin depth, the depth of investigation increases with the target conductivity and conductivity contrast and decreases with the detection threshold. Choosing a threshold mainly depends on the S/N ratio of the EM data if the sensor setup, data acquisition methods, and processing techniques are well established. A high threshold such as 20% or 30% is recommended for resistive targets or in areas where environmental noise is high or where terrain conductivity is low (<50 mS/m). In contrast, a threshold as low as 5% or 10% can be used for conductive targets in quiet areas. Field examples are presented to illustrate how to use the depth of investigation in data interpretation and presentation.

INTRODUCTION

Small, handheld, broadband electromagnetic (EM) sensors have many applications in investigating landfills, trenches, contaminant plumes, and structural foundations (Won et al., 1996; Won et al., 1997; Won 1998; Witten and Calvert, 1999; Huang and Won, 2000, 2003a, b; Witten et al., 2003; Smith et al., 2004). For many applications, the depth of investigation is of primary interest, particularly for small EM sensors having negligible separation between the transmitter and receiver coils. The term *depth of investigation* has evolved and become standardized (e.g., Spies, 1989) to mean the practical depth of investigation, defined as a maximum depth at which a given target in a given host can be detected by a given sensor. The skin depth has been widely used as an estimate of depth of investigation of EM systems, which is rigorously defined in classical EM theory as the distance in a homogeneous medium over which the amplitude of a plane wave is attenuated by a factor of $1/e$, or to about 37% of the original amplitude. The skin depth δ is

$$\delta = \sqrt{\frac{2}{\sigma\mu\omega}}, \tag{1}$$

where σ is the medium conductivity, μ is magnetic permeability, and ω is the angular frequency of the plane wave. In some geophysical textbooks, the term *depth of penetration* appears synonymously with skin depth. However, depth of investigation is clearly empirical; it is affected by the properties of the target and host medium as well as factors related to the investigation modality, such as sensor sensitivity, accuracy, frequency, coil configuration, ambient noise, and data processing and interpretation methods. Under ideal conditions, the depth of investigation can be greater than the skin depth. In geologically complex and/or environmentally noisy areas, however, the depth of investigation can be much less than the skin depth.

Manuscript received by the Editor October 15, 2003; revised manuscript received March 1, 2005; published online October 21, 2005.
[1]Geophex Ltd., 605 Mercury Street, Raleigh, North Carolina 27603-2343. E-mail: huang@geophex.com.

Schlumberger and Schlumberger (1932) first introduced the concept of depth of investigation for the nascent dc resistivity method. Evjen (1938) defines the depth of investigation as the depth at which a thin horizontal layer contributes the maximum amount to the total measured signal as measured on the ground surface. Since then, many authors have dealt with the subject for a variety of electrode arrangements and dc resistivity structures (e.g., Roy and Apparao, 1971; Barker, 1989). A similar concept for EM induction methods was pioneered by Doll (1949). Since then, Paul and Roy (1970) and Spies (1989) have studied this topic for ground EM systems, and Lakshmanan and Bichara (1981), Huang (1991), and Peltoniemi (1998) have researched it for airborne EM systems.

This paper specifically considers small, handheld, broadband EM sensors that are popular for mapping and imaging near-surface geophysical features when investigating environmental and geoengineering problems. Most traditional EM sensors have separate transmitter and receiver coils connected by cables. They also adopt a notion that the transmitter/receiver separation ultimately governs the depth of exploration — the farther they are apart, the deeper we can see. I show that a small sensor can explore considerable depths by using multiple frequencies. To quantify the depth of investigation for small sensors, I first present the factors affecting the depth of investigation and then analyze it using layered half-space models. I finally show field examples to illustrate how to use the depth of investigation in data display and interpretation.

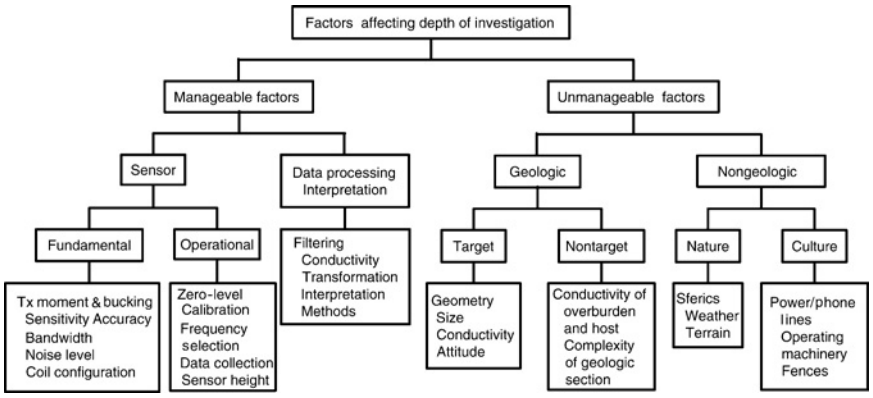

Figure 1. Factors affecting depth of investigation.

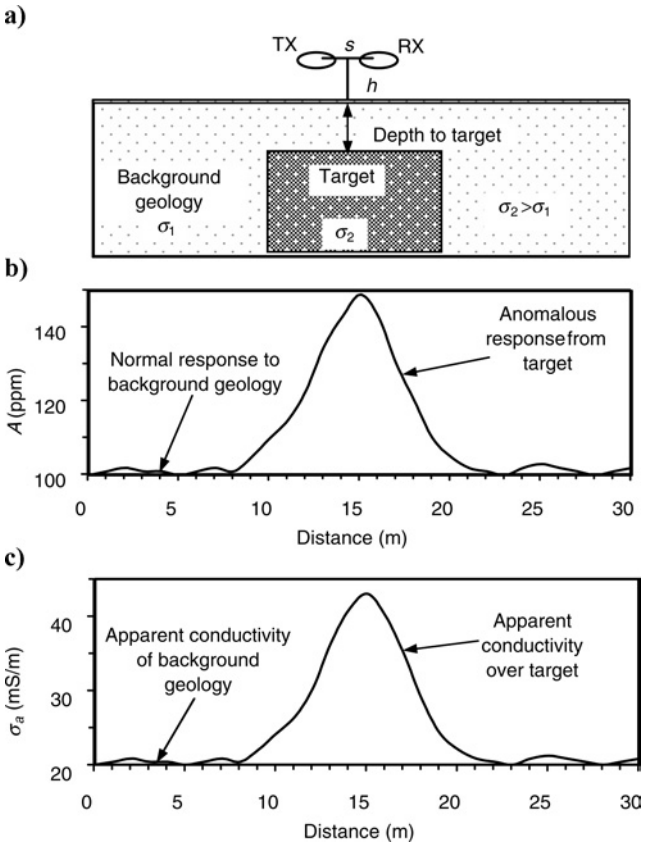

Figure 2. (a) Schematic representation of the problem. TX is transmitter; RX is receiver. (b) An EM amplitude anomaly over a target. (c) Apparent conductivity anomaly over a target.

FACTORS AFFECTING DEPTH OF INVESTIGATION

Figure 1 illustrates the complexity of the problem by first dividing the factors into two somewhat intrinsic categories: manageable and unmanageable. Manageable factors can be controlled or changed by the user, the sensor, and the survey modality; unmanageable factors are natural conditions that cannot be controlled or changed. One can always improve the manageable factors relating to the design and operation of the sensor as well as methods of data collection, processing, and interpretation. By advancing and optimizing the manageable factors, one hopes to derive the best methodologies to overcome the difficulties imposed by the unmanageable factors attributable to the target, geology, and environment.

The most important manageable factor is the instrument itself. In this paper, I use the GEM-2 (Won et al., 1996), a small, handheld, broadband sensor, for the purpose of discussing the depth of investigation. The GEM-2 is a fixed-geometry sensor but allows variable multiple-frequency operations suitable for depth sounding. A GEM-2 (Figure 2) has a transmitter-receiver coil separation s of 1.66 m and standard survey height h of 1 m. A third coil is used to monitor and cancel, or buck, the transmitter field. The sensor operates in a bandwidth from 30 Hz to 48 kHz. Raw data are the in-phase and quadrature components of the secondary magnetic field as parts per million (ppm) against the primary field at the receiver coil. The foremost incentive of a small, handheld sensor is its portability, survey speed, and easy use.

A sensor with a small coil separation can be used for depth sounding if it has (1) a method of canceling the strong transmitter field that exists at the receiver coil, (2) sufficient sensitivity and accuracy to resolve small changes in earth conductivity, (3) a large dynamic range to accommodate

near-surface effects, (4) a wide bandwidth to cover desired ranges in skin depth, and (5) an ability to avoid certain frequencies with high environmental noise levels caused by cultural sources such as powerlines. A sensor that can meet these requirements can be used for depth sounding in a variety of geological settings (Won, 2003). Since the measurements of EM sensors are usually in terms of the ratio of secondary to primary fields, increasing the transmitter moment does not change the receiver response. However, it does increase the secondary voltage induced in the receiver coil and thus raises the S/N ratio, which in turn can increase the depth of investigation.

Precise sensor calibrations are essential to obtain accurate data as indicated by Fitterman (1998), who describes several sources of calibration errors in helicopter EM data. The static EM zero level (instrument output when there is no target) slowly drifts, which is harmless for anomaly hunting but seriously distorts the phase of the data. The zero-level calibration is very important for converting EM responses to apparent conductivities or inverting to layered models (Huang and Won, 2000, 2003a). Any calibration error will drastically affect the depth image or soundings. Well-calibrated data help to bring out weak anomalies from deep targets that may not be obvious in raw data but often become pronounced in the interpreted results (Huang and Fraser, 1996; Huang and Won, 2003b).

There are three considerations in selecting operating frequencies: skin depth, signal level, and environmental noise. A low frequency yields large skin depth but low signal (induced-receiver-coil voltage) amplitude. As the frequency increases, the signal amplitude increases and the skin depth is reduced. In areas where the terrain conductivity is less than 50 mS/m (large skin depths), the frequency selection should be on the signal-level (high) side so as to obtain reliable data. The EM signal level is high in very conductive areas (>200 mS/m), where the main concern in choosing frequencies should be the skin depth. The GEM-2 sensor is able to measure environmental EM noise in the operating-frequency band, allowing one to choose the frequencies in the field and avoid using frequencies at which environmental noise is high.

Sensor height above the ground for a given coil separation is related to signal intensity for both the targets at depth and shallower surface geology. Large sensor height yields a larger relative response of the deeper target anomaly compared to the surface geology and so theoretically increases the depth of investigation. However, this increase of depth of investigation is limited by the reduction of the target signal level with the sensor height. For a handheld EM sensor like the GEM-2, the standard sensor height corresponds to the practical carrying height (about 1 m) and rarely changes much in practice, although some users tow it on a (nonmetallic) sled. Using caution in data acquisition may reduce noise related to geology and/or varying sensor height. For instance, over magnetic soils, in-phase components at lower frequencies may fluctuate with varying sensor heights (Huang and Won, 2004). Keeping the sensor at a constant height during a survey will reduce such noise.

Natural and cultural noise sources are obviously unmanageable. Natural EM noise comes from thunderstorms with lightning discharges that propagate globally through the ionosphere. Nearby lightning discharges produce randomly spaced events of short duration, called sferics, which can be filtered out to some extent. Distant discharges, however, are weaker, less distinct in amplitude, and more frequent; thus, they constitute a more-or-less steady background noise that has a strong frequency dependence (Palacky and West, 1991). Another natural source is from variations in the geomagnetic fields as a result of solar activity. These EM noise sources vary from place to place and from time to time. Cultural noise sources include powerlines, broadcasting airwaves, buried cables, pipelines, highways and railroads, and buildings, all of which may produce varying degrees of unwanted signals in the data. Close to the survey area, the most unmanageable factors are the properties of the target and the host medium. The most favorable case, needless to say, is when a conductive target of strong contrast is located in a resistive host medium.

Unlike the well-defined skin depth, there is no definitive way to determine the depth of investigation. Nonetheless, I attempt to formulate some simple rules based on simple models and the assumption that the manageable factors are optimized to an acceptable level. The analysis establishes the depth of investigation in terms of sensor frequencies, coil separation (manageable factors), medium and target conductivities (unmanageable factors), and detection threshold, which is related to the quality of the observed data.

DETECTION OF A HALF-SPACE BELOW A SINGLE LAYER

Many authors (e.g., Ward and Hohmann, 1988) deal with a layered half-space under a magnetic dipole source excitation at a distance h above the surface. The analysis may use the anomalous in-phase I and quadrature Q components or the amplitude $A = (I^2 + Q^2)^{1/2}$ and phase $\varphi = \tan^{-1}(Q/I)$ of the measured secondary magnetic field. Alternatively, one can use the apparent conductivity σ_a derived from I and Q (Huang and Won, 2000).

Figure 2 demonstrates schematically a target having a conductivity σ_2 embedded in a medium having a conductivity σ_1. We assume that the horizontal extent of the target is much greater than the transmitter-receiver coil separation and depth to the target so that it can be viewed as a layer or half-space. Let A_0 be the background response in the absence of the target; the apparent conductivity σ_a, computed from the background data, will be the same as σ_1. Over the target, we observe an anomalous response A_a and an apparent conductivity σ_a that would be between σ_1 and σ_2. A target is detected when the observed A_a/A_0 or σ_a/σ_1 is notably different from 1. To quantify this notability, let us specify a detection threshold T above the background. A target is detected when the observed A_a/A_0 or σ_a/σ_1 is greater than $1 + T$ or less than $1 - T$. In electrical and EM explorations, the detection threshold is usually 5% to 15%, depending upon data quality and the complexity of the geologic structures of interest (i.e., the noise envelope). A much higher threshold of 30% is used in the following discussions for the purposes of graphic presentation and to make a conservative estimate of the depth of investigation. Therefore, to find the depth of investigation in this case, we can increase the depth to the target and compute A_a/A_0 or σ_a/σ_1 until they are equal to $1 + T$ or $1 - T$. The depth at which the anomaly is equal to $1 + T$ or $1 - T$ should be the depth of investigation at a given threshold.

I then discuss how the depth of investigation is determined using two-layer models. As an example, Figure 3 shows a suite of curves for (a) the amplitude anomaly A_a/A_0 and (b) the apparent-conductivity anomaly σ_a/σ_1 as a function of depth to the target half-space t_1 for a case where the upper-layer skin depth δ_1 is 50 m. I first compute A_a and A_0 from the models and then invert the EM response to obtain σ_a (Huang and Won, 2000). The suite contains six graphs where the contrast σ_2/σ_1 varies by a decade from 0.001 to 1000. Two dotted lines indicate the bounds for the $T = 30\%$ detection threshold; the points where the dotted lines intersect graphs determine the depth of investigation. For instance, the depth of investigation is approximately 12 m for $\sigma_2/\sigma_1 = 100$, while it is about 3 m for $\sigma_2/\sigma_1 = 0.1$ (see the arrows). Either anomaly yields about the same depth of investigation, but the conductivity anomaly is somewhat more pronounced at higher contrasts.

The problem remains, however, that the depth of investigation depends on what one specifies for the detection threshold T. To study this, note Figure 4a, an amplified version of Figure 3b for two selected conductivity contrasts: $\sigma_2/\sigma_1 = 10$ and 1000. Notice that the depth of investigation is more sensitive to T when the conductivity contrast is smaller. Figure 4b shows the depth of investigation normalized to that at $T = 30\%$ for the skin depth δ_1 in the upper layer equal to 50 m; this graph may be used to determine correction coefficients to estimate the depth of investigation for different detection thresholds. This normalized depth of investigation has an empirical form

$$\varphi(T) = a + b\,ln(T), \tag{2}$$

where T is in percent, $a = 3.10$, and $b = 0.61$.

Figure 4c shows a suite of apparent conductivity curves versus the layer thickness for various coil separations s. Large coil separations produce increased depths of investigation and a more pronounced conductivity anomaly. Figure 4d shows the depth of investigation normalized to that for $s = 1.66$ m (for the GEM-2), for which the depth of investigation takes an empirical form:

$$\psi(s) = c + ds + es^2, \tag{3}$$

where $c = 0.84$, $d = 0.10$, and $e = -0.0015$. Note that the depth of investigation increases only about 20% as s increases from 0.2 m to 2 m, an interesting point for small, handheld sensors. Increasing coil separation or sensor height increases the depth of investigation but decreases the signal level. Therefore, increased depth of investigation is limited by the reduction in signal level from increasing the coil separation or sensor height.

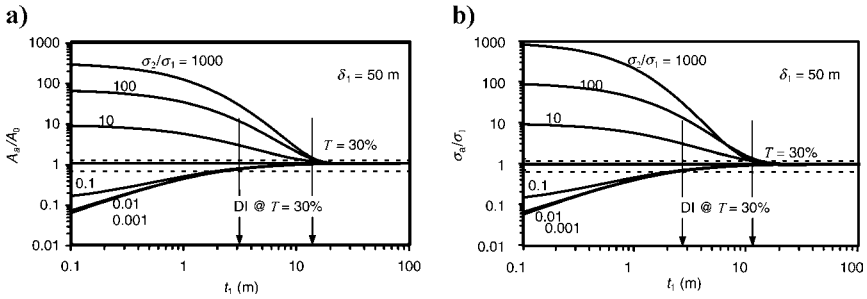

Figure 3. (a) Amplitude and (b) apparent conductivity curves as a function of depth to the buried half-space for a set of two-layer models. The skin depth is fixed at 50 m, and the conductivity contrasts between the two layers vary from 0.001 to 1000.

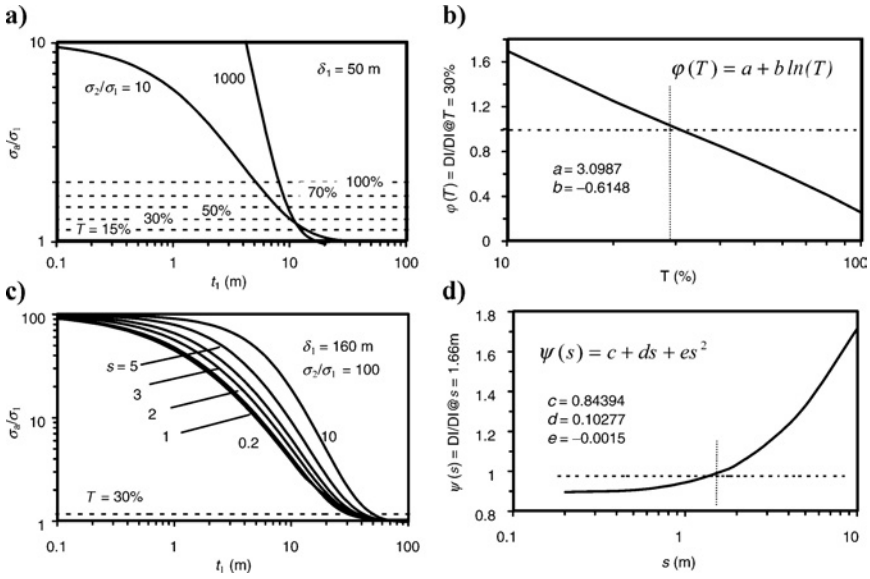

Figure 4. The depth of investigation for a buried half-space as functions of (a, b) detection threshold T and (c, d) coil separation s.

Figure 5a shows the relation between depth of investigation and skin depth in the upper layer δ_1 for various conductivity contrasts when $T = 30\%$. This figure is formed by merging many figures similar to Figure 3 for various skin depths. The dotted lines are computed from the amplitude A_a/A_0, while the solid lines are from the conductivity contrast σ_a/σ_1, both of which produce a similar depth of investigation. When the skin depth is small, the depth of investigation is almost independent of the contrasts. As the skin depth increases, the depth of investigation increases, but at a lesser rate for a resistive half-space than for a conductive basement. The depth of investigation is always smaller than the skin depth, as depicted in this graph.

Figure 5b presents the average depths of investigation for various conductivity contrasts shown in Figure 5a and background amplitudes A_0. It can be used as a graphic method to determine the depth of investigation for a given skin depth when $T = 30\%$. As an example, for $\sigma_1 = 0.01$ S/m, at 1 kHz the skin depth is 159 m, which corresponds to a depth of investigation of 14 m and A_0 of 40 ppm, as shown by the dotted lines in the figure. The estimate of the depth of investigation is valid only when the anomaly amplitude A_a is greater than 52 ppm or less than 28 ppm ($T = 30\%$), so that the anomalous response can be

measured reliably. The depth of investigation in this figure may be expressed as

$$\mathrm{DI} = \alpha\delta_1^{\beta} \approx \sqrt{\delta_1}, \tag{4}$$

where DI is the depth of investigation, $\alpha = 0.94$, and $\beta = 0.53$. Finally, considering equations 2 and 3, we have

$$\mathrm{DI} = \alpha\delta_1^{\beta}\varphi(T)\psi(s) \approx \sqrt{\delta_1}\varphi(T)\psi(s). \tag{5}$$

Notice that φ and ψ are simple multipliers as T or s varies. To estimate the depth of investigation from equation 5, we take four steps. First, we compute φ from equation 2 for a set detection threshold T. Then we compute ψ from equation 3 for a given coil separation s. Third, we determine the skin depth from the upper-layer conductivity and the sensor frequency. Finally, we obtain the depth of investigation from equation 5.

Setting a proper threshold T is the most imprecise part of the procedure; it depends on data quality as related to sensor construction, sensitivity, resolution, dynamic range, calibration, and noise level. As indicated above, a prerequisite for setting a detection threshold and thus estimating the depth of investigation is that all manageable factors presented in Figure 1 are acceptably established. Then, the noise level or S/N ratio in the survey area will be the main concern in determining the threshold. Conductive targets produce higher signal levels and more pronounced anomalies, allowing a lower threshold. However, a resistive target underlying a conductive overburden usually yields an ambiguous anomaly, so a higher threshold must be used. The threshold can be 5% to 10% under ideal circumstances — for example, a conductive target (>200 mS/m) in rural (low cultural noise) areas. In noisy urban areas, higher thresholds such as 20% or 30% are suggested to avoid overestimating the depth of investigation.

DETECTION OF A HALF-SPACE BELOW MULTIPLE LAYERS

The depth of investigation determined from equation 5 may be extended to a multilayered earth. Price (1949) first proposed the concepts of cumulative conductance and effective conductivity, and Spies (1989) uses them to estimate the depth of investigation for various EM systems. The cumulative conductance S down to depth of z is written as

$$S(z) = \int_0^z \sigma(z)dz, \tag{6}$$

where $\sigma(z)$ is the conductivity as a function of depth z. Then the effective conductivity at depth z is given by

$$\sigma_e(z) = \frac{S(z)}{z}. \tag{7}$$

In other words, we approximate the earth to the depth z as a single layer having a conductivity σ_e for which we have already derived the depth of investigation in equation 5.

The effective conductivity can be used to determine whether (1) a target half-space under a sequence of layers is detectable and (2) an interpreted layer obtained from an inversion (Huang and Won, 2003a) is supported by the data. As shown in Figure 6a, let us consider three layers above a very conductive basement. This model simulates a sequence of soil, shale, sandstone, and shale. The shale layers contain varying degrees of saltwater. To estimate the ability of the GEM-2 — for instance, to detect the basement of 1 S/m at 10 m depth — first compute S and σ_e. The rest follows the four steps outlined in the previous section. For Figure 6a, we have σ_e (10 m) = 0.24 S/m, which yields a depth of investigation of 10.9 m at 100 Hz for a 30% threshold.

When a target is interpreted to be deep, it is uncertain if its existence is supported by the data. We can use the same technique to estimate the depth of investigation. To illustrate the procedure, let us assume that the layering in Figure 6a is an interpreted result. We then calculate $S(z)$ and $\sigma_e(z)$ for successive depths as shown in Figure 6b. The depth of investigation values are then calculated by letting $\sigma_1 = \sigma_e(z)$ in equation 5. Figure 6c shows the depth of investigation at three frequencies. The intersections of each depth-of-investigation curve and a straight line $z = \mathrm{DI}$ indicate the depth of investigation for each frequency. Notice that the depth of investigation at 100 Hz is about 11 m, greater than the actual depth of 10 m, assuring that the data support the interpretation. The certainty of the depth of investigation thus determined can be estimated by the angle subtended by a depth-of-investigation curve and the straight line, which is large in a conductive layer and small in a resistive layer. The larger the angle, the higher the degree of certainty of the determined depth of investigation. The depth of investigation decreases rapidly in conductive layers and increases slowly in resistive layers, as shown in Figure 6c.

Finally, a data-quality check can be made. First, from the model one computes the response $A_a = 88$ ppm at 100 Hz. The target basement of the interpreted model is then replaced with the third layer to compute the background response $A_0 = 64$ ppm. This gives an anomaly of 24 ppm (37.5%); check the noise at 100 Hz and make sure it is less than 24 ppm.

FIELD EXAMPLES

A GEM-2 survey using frequencies of 4050 and 12 270 Hz was carried out to locate buried broken mirror pieces that cause lead contamination in groundwater. Huang and Won (2003a) performed an inversion to a layered model using data from a portion of a survey line to estimate depth to the buried

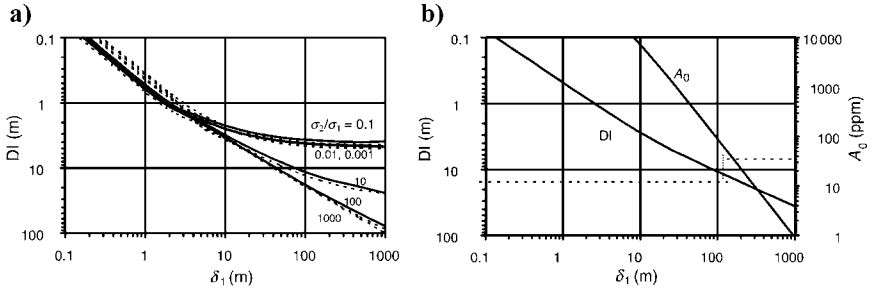

Figure 5. (a) The depth of investigation for a buried half-space as functions of δ_1 for various conductivity contrasts σ_2/σ_1 at a detection threshold of 30%. The solid curves are from apparent conductivity σ_a/σ_1, and the dotted curves are from the amplitude A_a/A_0. (b) The mean depth of investigation and normal amplitude of the EM response.

contaminants and possibly its vertical extent. Figure 7a and b shows two- and three-layer inversion results as a resistivity-depth section. Resistivity lows (or conductivity highs) in the middle of the section reflect the buried materials.

The depth of investigation calculated from the resulting models are indicated by white lines. As can be seen in Figure 7a, the depth of investigation for a detection threshold of 30% is located inside the basement, indicating it is successfully detected. For the three-layer model in Figure 7b, however, neither line, at either the 10% or the 30% threshold, reaches the third layer at the bottom, indicating that the second-layer thickness cannot be ascertained from the data. Final checks are made in measured amplitudes (Figure 7c). The background is the upper layer with infinite depth extent, and its response can be measured if the profile is long enough or it can be computed from the inverted model. Figure 7c shows the computed background (dashed lines). It is obvious that the measured anomalies are much higher than 30% of the background, reinforcing the validity of the two-layer model. The S/N ratio is very high in this example, so a lower detection threshold (5% or 10%) can be used.

The U.S. Geological Survey conducted a GEM-2 survey to characterize shallow brine contamination in Osage County, Oklahoma (Smith et al., 2004). The EM data at five frequencies from 330 to 47 010 Hz were collected using the GEM-2 sensor. Figure 8 shows the apparent-conductivity map derived from the in-phase and quadrature components at 13 590 Hz. The conductivity and gamma-ray logs were performed in the drill holes shown on the map. Also, dc soundings were carried out at some spots. Borehole measurements define shale units with high gamma-ray levels and moderate conductivity and brine with very high conductivity.

An inversion to a layered model was performed using the EM data obtained at line 2, which passes drill holes AA02 and AA03 (Figure 8). Figure 9 presents the inverted conductivity-depth section as well as results from the conductivity logs in the two drill holes and dc sounding near AA02. A very conductive layer is defined at depths of 2 to 3 m, which is the chloride concentration. The conductive layer from the inversion is slightly shallower than that from the logging and dc sounding. This can be caused by either system errors of the sensor or seasonal variation in chloride. The depths of investigation, even computed using a high threshold (e.g., 30%) are much greater than the depth of the chloride concentration zone. In fact, a much lower threshold can be used since the S/N ratio and target conductivity are high. For example, the depth of investigation at the highest frequency, 47 010 Hz, is shown on the color section in Figure 9a for a threshold of 10%.

A GEM-2 sounding was also carried out south of drill hole AA60 by holding the sensor and collecting the EM data continually for about 30 s. Figure 10 shows an inversion result from the sounding data. The input data to the inversion program utilized stacking of 280 samples, permitting use of a lower threshold to estimate the depth of investigation. Two chloride concentrations at depths of 4 and 13 m are indicated by the inversion. The shallow one matches the result from the conductivity logging, which is not available at depth. However, the dc sounding indicates that the conductivity is increasing at depth (Figure 10c).

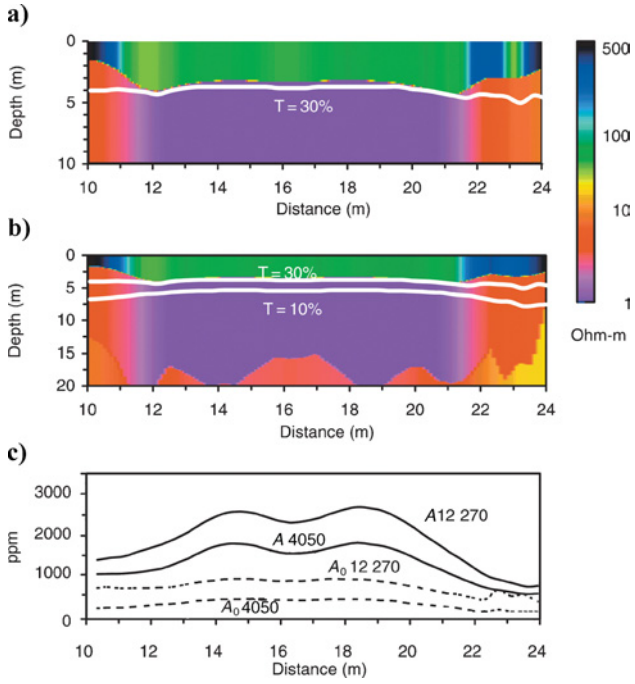

Figure 7. The resistivity sections obtained from (a) two-layer and (b) three-layer inversions. The white curves on the color sections are the depth of investigation for specific detection thresholds. (c) Measured EM amplitudes A (solid lines) at 4050 and 12 270 Hz and the computed amplitudes (dashed lines) A_0 of the normal background.

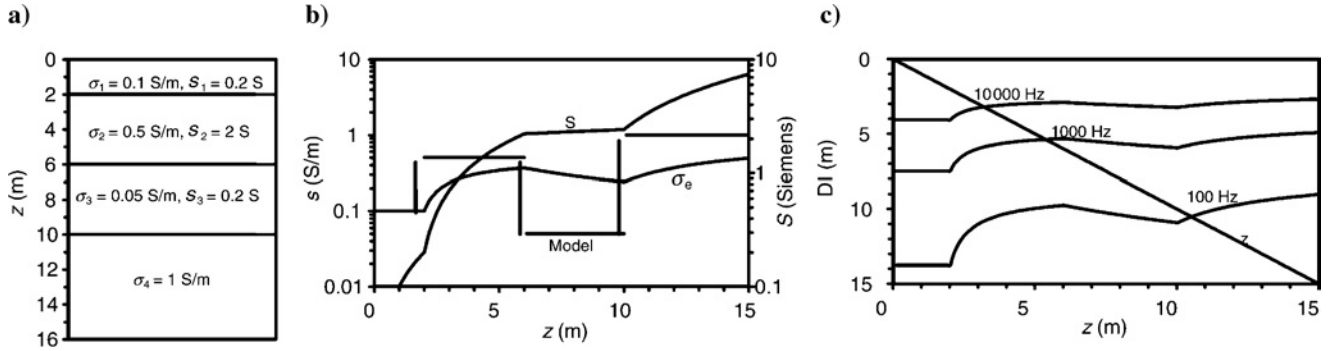

Figure 6. (a) A four-layer model study to determine the ability to detect the basement. (b) The associated cumulative conductance and effective conductivity. (c) The depth of investigation obtained for this model for three frequencies using a detection threshold of 30%.

The depths of investigation at the lowest frequency (330 Hz) are calculated for four thresholds (30%, 20%,10% and 5%) and are shown as crosses next to the vertical axis of Figure 10a. They increase from 11.7 m for $T = 30\%$ to 17.3 m for $T = 5\%$, indicating a deep chloride concentration zone. The amplitudes at the lowest frequency are 61 ppm for the layered half-space and 38 ppm for the background (the layer sequences above the lower conductive layer). Thus, the lower conductive layer produces a target-to-background anomaly of 60%. It seems that the resistive basement is detected based on the depth of investigation for the 5% threshold (17.3 m). As a matter of fact, the resistive basement in the interpreted model produces an anomaly much less than 5%, so its existence is not supported by the data. To present a meaningful inversion result, the depth in Figure 10a should not have exceeded 13 m.

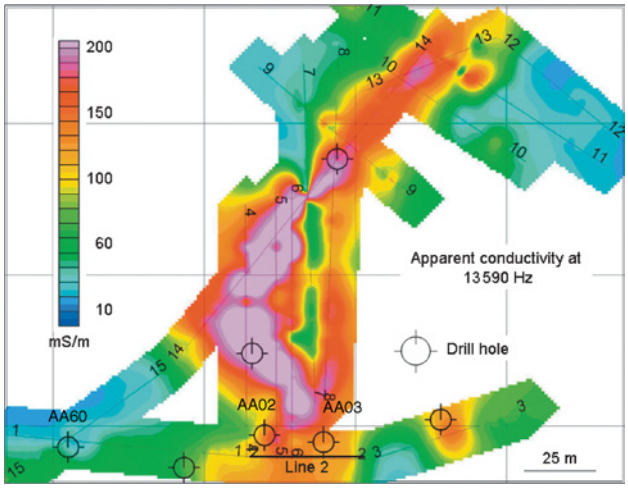

Figure 8. Map of the apparent conductivity (250 × 160 m) derived from the EM data at 13 590 Hz obtained in Osage County, Okalahoma. The drill-hole locations, survey lines, and respective numbers are also shown on the map.

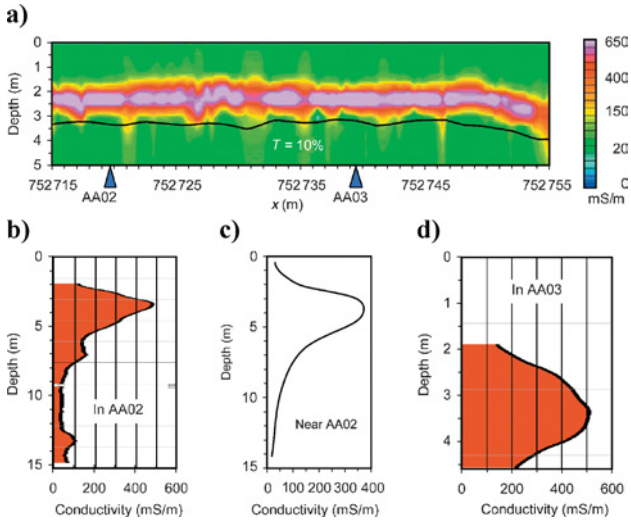

Figure 9. (a) The conductivity-depth section obtained from a layered-model inversion for line 2. (b) The results from conductivity logging in drill hole AA02. (c) The dc sounding near drill hole AA02. (d) The conductivity logging result in drill hole AA03. The depth of investigation at 47 010 Hz is shown on the color section for a threshold of 10%.

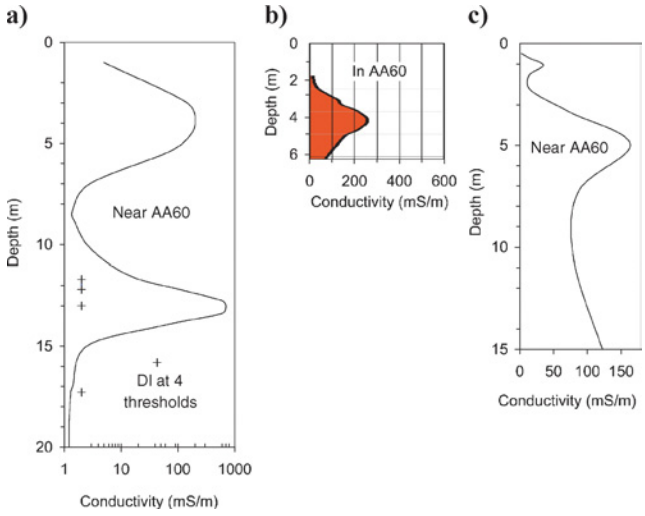

Figure 10. (a) The conductivity-depth section obtained from a layered-model inversion using the EM data obtained near borehole AA60, compared with the results from (b) the conductivity log and (c) the dc sounding.

CONCLUSIONS

Factors affecting the depth of investigation of EM sensors are grouped as manageable and unmanageable. One can improve manageable factors, including the sensor's sensitivity, accuracy, noise level, bandwidth, transmitter moment, and data acquisition and processing methods, to increase the depth of investigation. To estimate the depth of investigation for a handheld EM sensor, the GEM-2, I first considered a half-space buried under a single layer to derive empirical formulas. I then extended the analysis to an arbitrarily layered earth using the concept of cumulative conductance to replace it with an equivalent single layer, which is then applicable to the same formulas. For a given detection threshold and conductivity contrast between the target and host, the depth of investigation is approximately proportional to the square root of the skin depth in the host. The depth of investigation for a given skin depth increases with target conductivity and conductivity contrast, and it decreases with the detection threshold. Choosing a threshold is mainly dependent on the S/N ratio in the EM data if all the manageable factors are well established. I suggest that a high threshold, such as 20% or 30%, be used for resistive targets or in areas where environmental noise is high or terrain conductivity is low (<50 mS/m). In contrast, a threshold as low as 5% or 10% can be used for conductive targets in quiet areas.

ACKNOWLEDGMENTS

The author thanks I. J. Won and Bill SanFilipo of Geophex for their useful suggestions and language editing. The author also acknowledges Bruce Smith of the U.S. Geological Survey and two other anonymous reviewers for their important comments and suggestions.

REFERENCES

Barker, R. D., 1989, Depth of exploration of collinear symmetrical four-electrode arrays: Geophysics, **54**, 1031–1037.

Doll, H. G., 1949, Introduction to induction logging and application to logging of wells drilled with oil-base mud: American Institute of Mining, Metallurgical, and Petroleum Engineers Petroleum Transactions, 148–162.

Evjen, H. M., 1938, Depth factor and resolving power of electrical measurements: Geophysics, **3**, 78–95.

Fitterman, D. V., 1998, Sources of calibration errors in helicopter EM data: Exploration Geophysics, **29**, 65–70.

Huang, H., 1991, Evaluation of time-domain airborne electromagnetic prospecting for conductive ore bodies by depth penetration analysis: Mineral Resource & Geology, **5**, 50–53.

Huang, H., and D. C. Fraser, 1996, The differential parameter method for multifrequency airborne resistivity mapping: Geophysics, **61**, 100–109.

Huang, H., and I. J. Won, 2000, Conductivity and susceptibility mapping using broadband electromagnetic sensors: Journal of Environmental and Engineering Geophysics, **5**, no. 4, 31–41.

———, 2003a, Real-time resistivity soundings using a hand-held broadband electromagnetic sensor: Geophysics, **68**, 1224–1231.

———, 2003b, Detecting metal objects in magnetic environments by broadband electromagnetic method: Geophysics, **68**, 1877–1887.

———, 2004, Electromagnetic detection of buried metallic objects using quad-quad conductivity: Geophysics, **69**, 1387–1393.

Lakshmanan, J., and M. Bichara, 1981, Depth of penetration of airborne electromagnetics over stratified earth: 51st Annual International Meeting, SEG, Expanded Abstracts, 32.

Palacky, G. J., and G. F. West, 1991, Airborne electromagnetic methods, *in* M. N. Nabighian, ed., Electromagnetic methods in applied geophysics. — Applications, part B: SEG, 811–877.

Paul, P. A., and A. Roy, 1970, Approximate depth of penetration in EM dipole prospecting: PAGEOPH, **81**, 26–36.

Peltoniemi, M., 1998, Depth of penetration of frequency-domain airborne electromagnetics: Exploration Geophysics, **29**, 12–15.

Price, A. T., 1949, The induction of electric current in non-uniform thin sheets and shells: Quarterly Journal of Mechanics and Applied Mathematics, **2**, 283–310.

Roy, A., and A. Apparao, 1971, Depth of investigation in direct-current methods: Geophysics, **36**, 943–959.

Schlumberger, C., and M. Schlumberger, 1932, Depth of exploration attainable by potential methods of electrical exploration: American Institute of Mining, Metallurgical, and Petroleum Engineers Transactions in Geophysical Prospecting, **97**, 127–133.

Smith, B. D., J. K. Otton, R. A. Zielinski, M. M. Abbott, H. Huang, and A. J. Witten, 2004, Conductivity depth imaging of areas of shallow brine plumes at the USGS OSPER Site, Osage Co., Oklahoma: Presented at 11th International Petroleum Environmental Conference, Integrated Petroleum Environmental Consortium.

Spies, B. R., 1989, Depth of exploration in electromagnetic sounding methods: Geophysics, **54**, 872–888.

Ward, S. H., and G. W. Hohmann, 1988, Electromagnetic theory for geophysical applications, *in* M. N. Nabighian, ed., Electromagnetic methods in applied geophysics: SEG, 130–311.

Witten, A. J., and G. Calvert, 1999, Characterizing the distribution of near-surface solution channels using electromagnetic induction and ground penetrating radar: Journal of Environmental and Engineering Geophysics, **4**, no. 1, 35–43.

Witten, A. J., G. Calvert, B. Witten, and T. Levy, 2003, Magnetic and electromagnetic induction studies at archaeological sites in southwestern Jordan: Journal of Environmental and Engineering Geophysics, **8**, no. 3, 209–215.

Won, I. J., 2003, Small frequency-domain electromagnetic induction sensors: The Leading Edge, **22**, 320–322.

Won, I. J., D. Keiswetter, G. Fields, and L. Sutton, 1996, GEM-2: A new multifrequency electromagnetic sensor: Journal of Environmental and Engineering Geophysics, **1**, no. 2, 129–137.

Won, I. J., D. Keiswetter, D. Hanson, E. Novikova, and T. Hall, 1997, GEM-3: A monostatic broadband electromagnetic induction sensor: Journal of Environmental and Engineering Geophysics, **2**, no. 1, 53–64.

Won, I. J., D. Keiswetter, and E. Novikova, 1998, Electromagnetic induction spectroscopy: Journal of Environmental and Engineering Geophysics, **3**, no. 1, 27–40.